Underactuated Adaptive Gripper Using Flexural Buckling

Gwang-Pil Jung, *Student Member, IEEE*, Je-Sung Koh, *Student Member, IEEE*, and Kyu-Jin Cho, *Member, IEEE*

***Abstract*—In gripping devices, adapting to highly unstructured environments such as irregularly shaped objects and surfaces continues to be challenging. To achieve safe and reliable gripping, many researchers have employed various underactuated mechanisms such as differential and compliant mechanisms. All these mechanisms have demonstrated successful gripping performances. They, however, have hardly considered scalability issues of underactuated mechanisms originating from additional force transmissions and onerous mechanism assembly. In this paper, we propose a structurally simple and scalable underactuated mechanism. The mechanism is demonstrated on a gripping device called the "Buckling gripper." The Buckling gripper achieves adaptive gripping on rugged, uneven, and undulating surfaces typically found in the natural world. The key design principle of the Buckling gripper is inspired by a caterpillar's proleg that highly deforms depending on the shape of the contact surface. This key principle is applied to the gripper via flexural buckling. Normally, buckling is avoided in mechanical designs, but the buckling behavior of a flexure with an adequately selected length provides wide gripping range with a narrow range of force variation, which provides a sufficient number of contacts with even contact forces. As a result, the Buckling gripper achieves adaptive gripping on various surfaces, similar to a caterpillar.**

***Index Terms*—Adaptive gripper, bioinspired robot, compliant gripper, flexural buckling, soft robot, underactuated gripper.**

I. Introduction

GRIPPING a variety of objects—from flat to wavy surfaces and irregularly shaped objects—essentially requires adaptability for safe and reliable gripping performance. For achieving high adaptability, many researchers have employed various underactuated mechanisms such as differential and compliant mechanisms. These mechanisms offer high adaptability by satisfying two conditions: a large number of contacts and even contact forces. Making a sufficient number of contacts is the primary purpose of underactuated mechanisms. However, if the object is in a situation in which contact force is concentrated on just one contact, the gripping will quickly become unstable [1].

Of the various underactuated mechanisms in macroscale, the differential mechanism has been widely employed in applications such as robotic hands [2]–[9] and mobile robots [10], [11]. The differential mechanism consists of one force input and two force outputs. When an external force is exerted on one output, the displacement of the other is in such a way that the output forces are equal. By stacking the mechanisms, the user is able to create a large number of outputs. As a result, the differential mechanism provides a sufficient number of contacts with even contact forces. Dollar and Howe used a moving pulley and tendon cables to actuate the fingers and grasp various objects [9]. Gosselin *et al.* proposed an anthropomorphic robotic hand with 15 degrees of freedom operated by a single actuator using differential mechanisms. Kim *et al.* employed a two-stage differential system in the toes of the Stickybot to conform to uneven surfaces and distribute the contact forces [11]. Compliant mechanisms also have been applied to many gripping devices [12]–[16]. The key is using adequately adjusted compliance of the materials to reliably adapt to the unstructured environments. Kim *et al.* analyzed stiffness of flexures to increase the spine attachments and load sharing ability [12]. Festo's FinGripper used two flexible bands so that they adapts to the irregularly shaped objects with gentle lateral forces [16]. In addition, other researchers have proposed novel underactuated mechanisms such as using granular materials [17] and pneumatic networks (PneuNets) of channels in elastomers [18]. These proposed underactuated mechanisms have shown success in grasping irregularly shaped objects, but they hardly have focused on scale-down issues originating from onerous mechanism assembly and additional force transmissions—differential mechanisms require additional force transmissions composed of linkages, joints, pulleys, etc.

In microscale, the compliant mechanism has been widely employed [19]–[23]. Basically, the compliant mechanism reduces assembly process and uses deflection of compliant beams as force transmissions, which is an appropriate property for small scale. Dechev *et al.* used deflection of compliant beams to grip and assemble microparts [19]. Krecinic *et al.* employed comb-like silicon skeletons to provide a large gripping stroke while reducing out-of-plane motion [21]. Hoxhold and Büttgenbach fabricated the flexible gearing to achieve a robust and powerful gripping mechanism [22]. Those compliant mechanisms have provided solutions in microscale gripping, but they have focused on the gripping motion itself and have hardly considered even force distribution among the contact points, which could induce safety and stability issues.

Manuscript received September 22, 2012; revised March 17, 2013; accepted July 3, 2013. Date of publication August 8, 2013; date of current version December 2, 2013. This paper was recommended for publication by Associate Editor J. Dai and Editor B. J. Nelson upon evaluation of the reviewers' comments. This work was supported by the Research Center Programs through the National Research Foundation of Korea funded by the Ministry of Education, Science, and Technology under Grant 2009-0087640 and Grant 2009-0082824. (Corresponding author: K.-J. Cho.)

The authors are with the Biorobotics Laboratory, School of Mechanical and Aerospace Engineering/Institute of Advanced Machinery and Design, Seoul National University, Seoul 151-916, Korea (e-mail: ceaser97@snu.ac.kr; kjs15@snu.ac.kr; kjcho@snu.ac.kr).

Color versions of one or more of the figures in this paper are available online at http://ieeexplore.ieee.org.

Digital Object Identifier 10.1109/TRO.2013.2273842

Fig. 1. Buckling gripper—dimensions of 15 mm × 10 mm × 6 mm and weight of 140 mg—attached to a cement block weighing 3 g (note that the tested cement block had surface waviness of 583.93 μm, which is more than six times surface roughness of normal concrete). The flexures of each spine show different bending angles since they adapt to the wavy surface (see the circles in the figure).

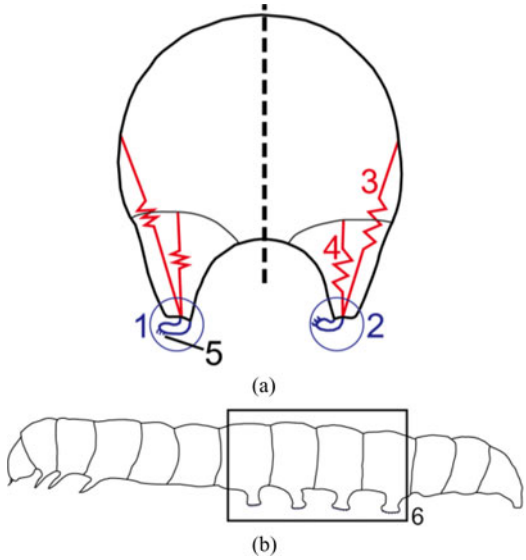

Fig. 2. (a) Diagrammatic section of caterpillar. (b) Lateral view of a *Carpocapsa pomonella* [24].

In this paper, we propose a biologically inspired simple and scalable underactuated mechanism for mesoscale applications. To demonstrate the mechanism, we apply a gripping device called a Buckling gripper. The Buckling gripper achieves adaptive gripping on rugged, uneven, and undulating surfaces typically existing in nature. Key design principles are adopted from the proleg in the abdominal segments of a caterpillar. Caterpillars accomplish robust gripping on most natural surfaces. Its key principles are its simple structure and the relatively soft cuticle attached to the tip of the proleg. These two key design principles—i.e., the simple structure and the highly deforming soft cuticle—are applied to the Buckling gripper via flexural buckling.

The behavior of flexural buckling offers a novel type of adaptive mechanism. In fact, buckling is normally considered to be failure and tends to be avoided in mechanical designs. When a flexure with an adequately selected length undergoes buckling, however, all spines are decoupled, and therefore, each spine moves more independently and adapts to the target surface. Flexural buckling also provides constant force for a certain range of deflection, which enables all the spines to have even contact forces.

From a structural viewpoint, the Buckling gripper is fairly simple. The fabrication process of the Buckling gripper begins from a single sheet patterned by laser machining, and therefore, the flexures where buckling occurs are naturally embedded as a part of the gripping structure. The fabricated Buckling gripper is shown in Fig. 1.

In the following sections, design, modeling, fabrication, and experiments are carried out. We modeled the buckling behavior of flexures by using the pseudorigid-body 3R model [32]. The model provides useful information to determine adequate length of the flexure. Several experiments are done to show how flexure buckling influences gripping performance. Gripping performance is tested on cement blocks that have random surface waviness and evaluated by investigating the number of contacts and measuring the holding force. In addition, a prototype is built to demonstrate adaptive gripping on various natural surfaces such as a brick, stone, and a tree.

II. Biological Inspiration and Concept Design

A. Biological Inspiration

Caterpillars climb rough and rugged surfaces using the prolegs of their abdominal segments, as shown in Fig. 2. A caterpillar's abdominal segment has a fairly simple structure. The overall shape of one abdominal segment is a closed curve. A pair of prolegs sticks out from both sides of the body and then inclines toward the ground, which allows a caterpillar to easily grip a target object, as shown in Fig. 2(a). Most caterpillars have four or five abdominal segments (6) that are connected back-to-back in series, as shown in Fig. 2(b).

Functionally, the abdominal segment is divided into a hydroskeleton body and the planta at the tip of each proleg. The hydroskeleton body is surrounded by cuticle and hydrostatic pressure, and tissue pressure provides the stiffness for muscle actuation [25]. The retractor muscles (3, 4) are attached to the inner side of the body wall. The other end of the retractor muscles is connected to the planta (1, 2), which makes it possible for the caterpillar to create stable, powerful, and passive attachments. The planta, which is attached to the end of each proleg, is made of relatively soft and opaque cuticle. The planta bears crochets (5) and gives compliance to the proleg, permitting great deformation [26]. By using its passive compliance and crochets,

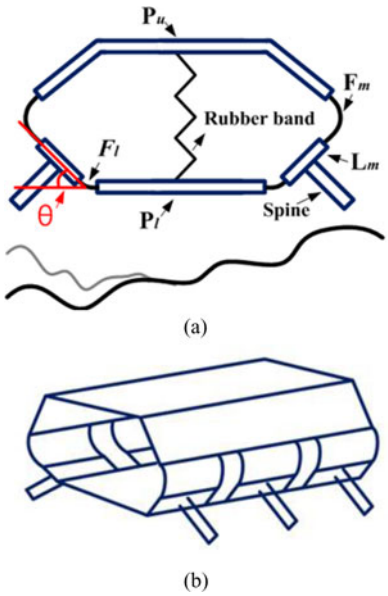

Fig. 3. (a) Basic gripping structure. (b) Multiple segments.

a caterpillar can maintain a robust grip on rough and rugged surfaces.

In addition, the mechanism of actuation is simple and energy efficient. Caterpillars control their planta by using contraction and release of the retractor muscles (3, 4). Initially, the planta is closed as shown on the right in Fig. 2(a). When the retractor muscles are contracted, the planta opens as shown on the left in Fig. 2(a). After releasing the retractor muscles, the planta closes again and grips the target object. In other words, caterpillars do not consume energy while maintaining the grasp.

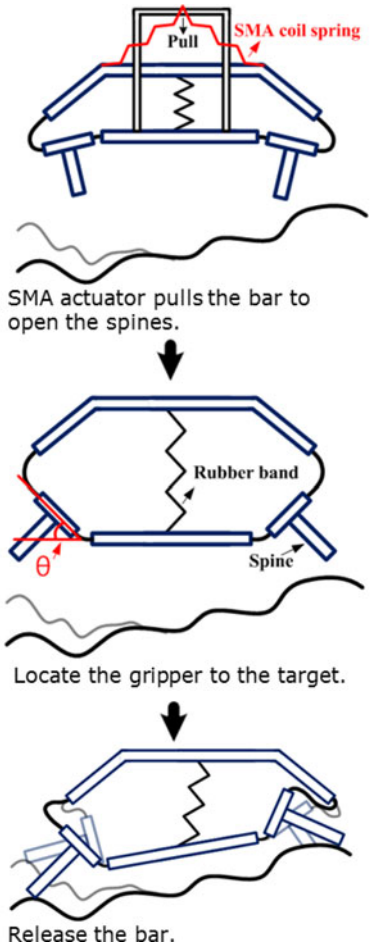

Fig. 4. Procedure of gripping: pushing the bar, locating the gripper on the place where attachment is desired, and releasing the bar.

B. Design

The overall shape of the Buckling gripper is inspired by the design of the caterpillar's prolegs in the abdominal segments. The gripper is made of rigid links and flexures, and a pair of spines sticks out from both sides, as shown in Fig. 3(a). The gripper has, from the top, an upper rigid plate P_u, whose two outer planes are bent toward the ground so that the spines face downward, and a lower rigid plate P_l. The upper plate and lower plate are connected by pairs of flexure links that are attached symmetrically on both sides of the plates. The spine link provides serial connection of the middle flexure joint F_m, the middle rigid link L_m where the spine is attached, and the lower flexure joint F_l. Inside the structure, a bar and two shape memory alloy (SMA) coil spring actuators are inserted for actuation and a rubber band is installed for recovery. The gripping motion is straightforward and the procedure is explained in Fig. 4.

The basic structure has a single pair of *spine links*. The single-paired gripper is extended to a gripper that has multiple pairs of spines, to increase the probability of successful gripping by increasing the number of contact points. The current design easily allows for the number of spines to be increased by connecting each pair back-to-back in series, as shown in Fig. 3(b). Then, all the *spine links* share the same upper and lower plates. Increasing the number of pairs without increasing the number of actuators, however, does not necessarily guarantee successful gripping.

There are two issues: One is that since the *spine links* are attached to the same upper and lower plates, the configuration of each spine is constrained. Second is that the force on each spine could differ depending on the position of the spine; one of the spines could apply a large force on the surface, and the gripping will easily be unstable. To increase the stable gripping probability, each spine has to make a contact with even forces on the contact points. Normally, differential mechanism is used for other grippers to solve this problem by providing the uniform contact forces. Differential mechanisms, however, are complicated to apply in small scale and have limited scalability. To solve this issue, we propose using the behavior of flexural buckling.

The behavior of flexural buckling displays a property of nonlinear force versus gripping angle. The gripping angle θ is indicated in Fig. 5(b). For example, let us assume that two grippers attach to a rugged surface shown in Fig. 5(a) and (b). One gripper has linear elastic materials, and the other has buckling flexures. When they attempt to attach to the rugged surface, each spine deforms by a different amount depending on the shape of the surface [see Fig. 5(a) and (b)].

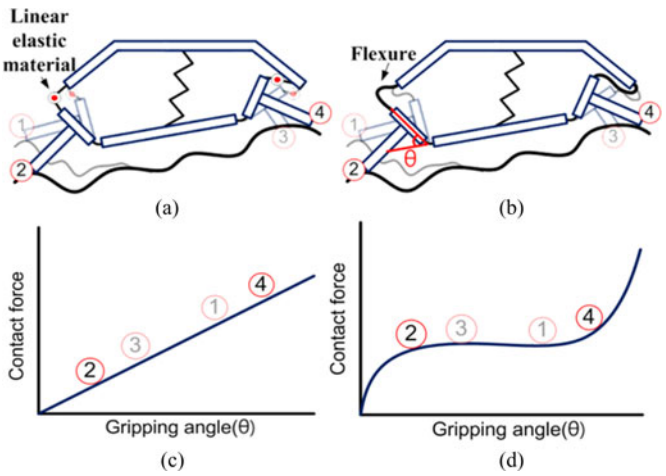

Fig. 5. Gripper with (a) linear elastic materials and (b) buckling flexures trying to grip the target surface; contact force versus gripping angle of the spines in the case of (c) linear force for linear elastic materials and (d) nonlinear force profile for buckling flexures.

In the case of a linear elastic material, the contact force is proportional to the gripping angle of each spine. Then, each spine has different contact forces depending on the deflection of the material, as shown in Fig. 5(c). Therefore, if one of them deflects more, the contact force is concentrated on the spine. As a result, the gripping posture may become unstable.

On the other hand, the behavior of flexural buckling displays a property of nonlinear force versus gripping angle, as shown in Fig. 5(b). This nonlinear property implies that the force remains constant for a certain range of deflection, and hence, all the spines will have similar contact forces. In other words, even though the contact force of each spine depends on and differs from their configuration, the constant force region allows the spines that are bent by different angles to generate identical contact forces, as shown in Fig. 5(d).

III. Contact Force and Gripping Range Analysis

The contact force and the gripping range of the Buckling gripper are determined by its flexures. The Buckling gripper includes two flexures (L_2 and l). The lower flexure l is related to the *force level*, but its main function is as a rotational joint. On the other hand, the middle flexure L_2, which undergoes buckling, is related to all the characteristics. Therefore, the length of L_2 is the main parameter to be considered when determining the characteristics of the Buckling gripper.

To analyze large and nonlinear deflections such as buckling, the pseudorigid-body model (PRBM) [27] is used. The PRBM provides a simple, straightforward method to analyze compliant mechanisms by replacing a flexure beam with a flexural pivot and a pseudorigid link. The force–deflection relationship is then determined by the principle of virtual work.

A. Modeling of Flexures

Several PRBMs have been developed to analyze the tip deflection of large deflecting beams for various loading conditions [28]–[31]. Among others, we applied the PRB3R model proposed by Su [31], which provides the constant spring stiffness and the constant geometric parameters that are independent of the loading condition. Generally, the characteristic radius factor and stiffness coefficients are dependent primarily on the external loading condition. In particular, these parameters show a large difference between two loading conditions: the pure force condition and the pure moment condition. Su computed the parameters under both conditions and optimized the parameters so that the tip deflection could fit well for a wide range of external loads. The optimized characteristic radius factor γ_n and the stiffness coefficients $K_{\theta n}$ are presented in Table I. Based on the values in Table I, the locations of the torsion springs and spring constants are determined. Fig. 6 shows the gripper and application of the equivalent model, the PRB3R model. The PRB3R model consists of four rigid links connected by three torsional springs. The stiffness of the three torsional springs placed at the pivot is given as $k_n = K_{\theta n} EI/L_2$, where E is young's modulus, and I is moment of inertia. The short flexure l is replaced with a short flexural pivot. The short flexural pivot is applied when the flexure is shorter than one tenth of the rigid part and when the stiffness of the torsional spring is given as $k_4 = EI/l$.

TABLE I
Characteristic Radius Factor and Stiffness Coefficient

Characteristic radius factor	$\gamma_1 = 0.1$	$\gamma_2 = 0.35$	γ_3=0.40	$\gamma_4 = 0.15$
Stiffness coefficient	$K_{\Theta 1} = 3.51$	$K_{\Theta 2} = 2.99$	$K_{\Theta 3} = 2.58$	

B. Static Gripping Force

To simplify the analysis, we make the following assumptions: First, the lower plate and upper plate move along the vertical direction. Second, the direction of the contact force is perpendicular to the spine. Third, generalized coordinates q are chosen for the actuation displacement $q_1 = d$ and the gripping angle $q_2 = \theta$. With these assumptions, we determine the contact force, actuation force, and other geometric properties such as θ_1, θ_2, and θ_3 by the principle of virtual work.

The kinematic coefficients are given in Table II, determined using the position vector closure equation and Cramer's rule.

Work done by the spine is given as

$$\delta W_s = \vec{F}_s \cdot \delta \vec{z}_s = F_s L_s \delta\theta. \tag{1}$$

Work done by the actuator is given as

$$\delta W_a = \vec{F}_a \cdot \delta \vec{z}_a = F_a \delta d. \tag{2}$$

Virtual work done by the torsional spring is given as

$$P.E. = \frac{1}{2}k_1\theta_1^2 + \frac{1}{2}k_2\theta_2^2 + \frac{1}{2}k_3\theta_3^2 + \frac{1}{2}k_4\theta^2 \tag{3}$$

$$\delta W_{\text{torsional}} = \sum \frac{\partial P.E.}{\partial q}(-\delta q). \tag{4}$$

Net virtual work done by the applied forces is given. Then, the following equation is valid:

$$\delta W_{\text{all}} = \delta W_s + \delta W_a + \delta W_{\text{linear}} + \delta W_{\text{torsional}} = 0. \tag{5}$$

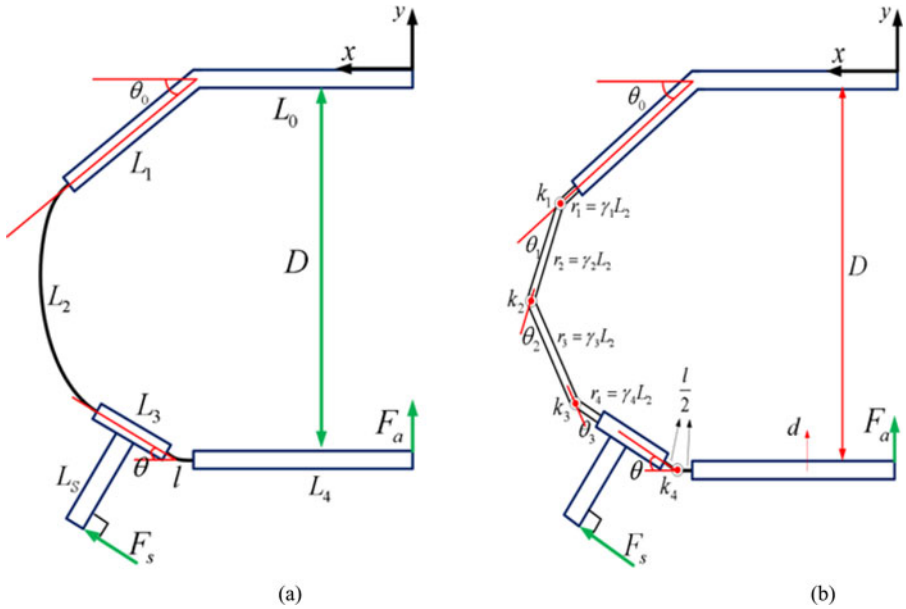

Fig. 6. (a) Gripper. (b) Its equivalent model. The bending angle θ_0 is a fixed value and is related to the initial shape. The long flexure L_2 where buckling occurs is modeled with four rigid links with lengths of r_1, r_2, r_3, and r_4. These lengths are determined by the characteristic radius factor given in [31, Tab. 2]. Three torsional springs are located between the links. The spring constants are k_1, k_2, and k_3, and the deflection angles are θ_1, θ_2, and θ_3. The short flexure l that performs a simple rotational joint is modeled with two rigid links and one torsional spring [27]. Lengths of both these links are equal to $l/2$, and the spring constant is k_4.

TABLE II
KINEMATIC COEFFICIENTS

$\frac{\partial\theta_1}{\partial q}$	$\frac{\partial\theta_2}{\partial q}$	$\frac{\partial\theta_3}{\partial q}$
$\frac{\partial\theta_1}{\partial d} = -\frac{1}{r_2}\frac{\sin(\theta_0+\theta_1+\theta_2)}{\sin\theta_2}$	$\frac{\partial\theta_2}{\partial d} = \frac{1}{r_3}\frac{\sin(\theta_0+\theta_1)}{\sin\theta_2} + \frac{1}{r_2}\frac{\sin(\theta_0+\theta_1+\theta_2)}{\sin\theta_2}$	$\frac{\partial\theta_3}{\partial d} = -\frac{1}{r_3}\frac{\sin(\theta_0+\theta_1)}{\sin\theta_2}$
$\frac{\partial\theta_1}{\partial\theta} = -\frac{r_4+L_3+l/2}{r_2}\frac{\sin\theta_3}{\sin\theta_2}$	$\frac{\partial\theta_2}{\partial\theta} = \frac{r_4+L_3+l/2}{\sin\theta_2}\left(\frac{\sin(\theta_2+\theta_3)}{r_3} + \frac{\sin\theta_3}{r_2}\right)$	$\frac{\partial\theta_3}{\partial\theta} = -1 - \frac{r_4+L_3+l/2}{r_3}\frac{\sin(\theta_2+\theta_3)}{\sin\theta_2}$

TABLE III
NORMALIZED PARAMETERS

Normalized parameter	Normalized parameter
$f_s = \frac{L_2^2}{EI}F_s$	$l_3 = L_3/L_2$
$f_a = \frac{L_2^2}{EI}F_a$	$l_s = L_s/L_2$
$l_1 = L_1/L_2$	$l' = l/L_2$
$d' = d/L_2$	-

By substituting (1)–(4) into (5) and grouping the equations depending on δq_i, we obtain the following equations:

$$f_s l_s - \left(k_{\theta_1}\theta_1\frac{\partial\theta_1}{\partial\theta} + k_{\theta_2}\theta_2\frac{\partial\theta_2}{\partial\theta} + k_{\theta_3}\theta_3\frac{\partial\theta_3}{\partial\theta} + \frac{1}{l'}\theta\right) = 0 \quad (6)$$

$$f_a - \left(k_{\theta_1}\theta_1\frac{\partial\theta_1}{\partial d'} + k_{\theta_1}\theta_2\frac{\partial\theta_2}{\partial d'} + k_{\theta_1}\theta_3\frac{\partial\theta_3}{\partial d'}\right) = 0. \quad (7)$$

The normalized parameters are given in Table III. The geometric relations are derived as

$$\theta_0 + \theta_1 + \theta_2 + \theta_3 + \theta = \pi \quad (8)$$

$$(\gamma_1+l_1)C_0 + \gamma_2 C_{01} + \gamma_3 C_{012} + (\gamma_4+l_3+l'/2)C_{0123} = 0 \quad (9)$$

$$(\gamma_1+l_1)S_0 + \gamma_2 S_{01} + \gamma_3 S_{012} + (\gamma_4+l_3+l'/2)S_{0123} = d'. \quad (10)$$

By solving (6)–(10) numerically, we can determine the contact force F_s, actuation force F_a, and other geometric properties $\theta_1, \theta_2, \theta_3$. Note that the contact force F_s is determined by solving (8)–(10) and (6). Note also that the input is the gripping angle θ and that the actuation displacement d is fixed.

The derived equations (6)–(10) consist of the parameters normalized by the upper link (L1 in Fig. 6). Therefore, several desired Buckling grippers that have same properties but various sizes can be developed by matching the length ratio—the length ratio indicates the ratio of the length of the flexures and the links (L2, L3, l in Fig. 6) to the length of the upper link (L1 in Fig. 6).

IV. FABRICATION

The gripper was fabricated using a smart composite microstructure (SCM) [32]. The SCM process replaces the

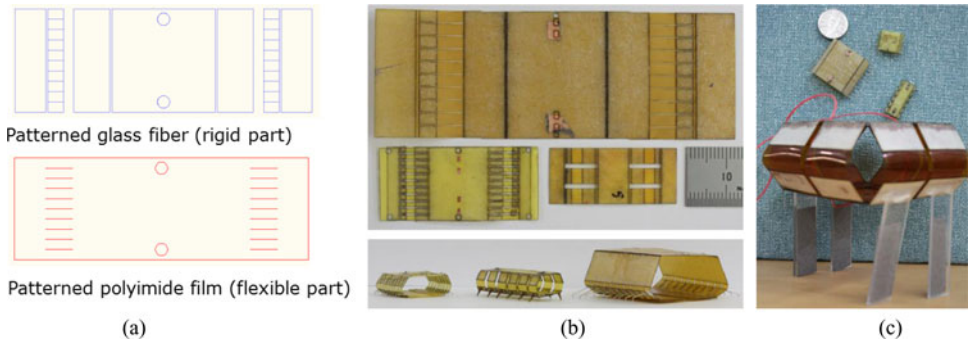

Fig. 7. (a) Two-dimensional pattern design. Circle-shaped holes are designed in order to install a rubber band through the gripping structure. Grippers are fabricated with varying lengths of the middle flexure joint. (b) Fabricated grippers of various scales and have the length ratios 0.714, 0.571, and 0.143. (c) Assembled grippers, ranging from a small gripper to a gripper the size of a human hand.

metal-based pin joints and links with composite-based links and flexure joints [33], [34], which makes it possible for the gripper to be small, compact, and lightweight. The gripping structure is divided into a rigid link part and a flexure joint part. The rigid links are made of glass fiber prepreg, and the flexure joints are made of polyimide film, as shown in Fig. 7(a). The assembly process consists of folding, spine attachment, and actuator insertions. Currently, all the assembly process is manually done, and therefore, robustness of the structure depends on the quality of the material and manufacturing.

For prestress in the structure, a rubber band is inserted between the upper and lower plates. As the stiffness of the rubber becomes larger, the contact force increases since the upper and lower plates get closer. The inserted rubber band has 20.1-g/mm stiffness. To open the spines, two symmetrically arranged SMA coil spring actuators are inserted between the upper plate and the bar [35], [36]. The actuator has 18 active coils of 13.6-g/mm stiffness in austenite phase, which is enough to actuate the rubber band.

In addition, users can easily change the size of the gripper depending on their desired properties; the properties—gripping range and contact force—of the Buckling gripper depend on the geometry, e.g., length ratio of the links and flexures. Fig. 7(b) and (c) shows fabricated grippers that differ in size and number of spines.

V. Results

The buckling behavior of the flexure may or may not enhance gripping performance, since the buckling behavior varies greatly with the length of the flexure [37]. To investigate the influence of the flexure length, we present the contact force measurements from the gripping experiments and the simulation results while varying the flexure length. Other simulations are done to investigate the characteristics, e.g., *gripping range*, *force level*, and *force variation*, under other actuation displacements.

To quantify the gripping performance, we perform gripping tests with artificial blocks that have controlled waviness while measuring the holding force. In addition, experiments are done with cement blocks that have random waviness to show the feasibility of the gripper on real natural surfaces. Finally, simple gripping tests are done on various other natural surfaces, e.g., a tree, stone, and brick.

A. Behavior of Flexural Buckling

To investigate the differing behaviors of the flexural buckling, we constructed an experimental setup that measures the contact force of various flexures with respect to the gripping angle. Fig. 8(a)–(c) shows the setup for measuring the forces of the gripper. Detailed geometrical properties of the tested grippers are provided in Table IV. The length ratio of the tested flexures is limited to the compression dominant loading condition since the employed compliant beam model fits well in moment dominant loading conditions [31].

Fig. 8(d) shows the change in contact force as the gripping angle θ increases according to the length ratio of the middle flexure. First, a nonlinear region appears where the local maximum and the local minimum exist, which is typical behavior of flexural buckling.

To characterize the buckling behavior, we propose three parameters, which represent the main differences between the short flexures and the long flexures: *gripping range*, *force level*, and *force variation*.

The *gripping range* is defined as

$$R_G = \theta_{\max} \tag{11}$$

i.e., the maximum gripping angle by which each spine can rotate independently. When the flexure is short, the gripping range becomes constrained by the length of the flexure itself, which inhibits additional rotation. That is, each spine moves more independently as the flexure increases in length.

The *force level* is defined as

$$F_L = \frac{1}{\theta_{\max}} \int_0^{\theta_{\max}} f_c(\theta) d\theta \tag{12}$$

where $f_c(\theta)$ is the function of the contact force. The *force level* is a representative contact force defined as an average of contact forces. The *force level* is related to the stiffness of the flexure, and therefore, the *force level* decreases as the length of the flexure increases. In Fig. 8(d), as the length ratio of the flexure

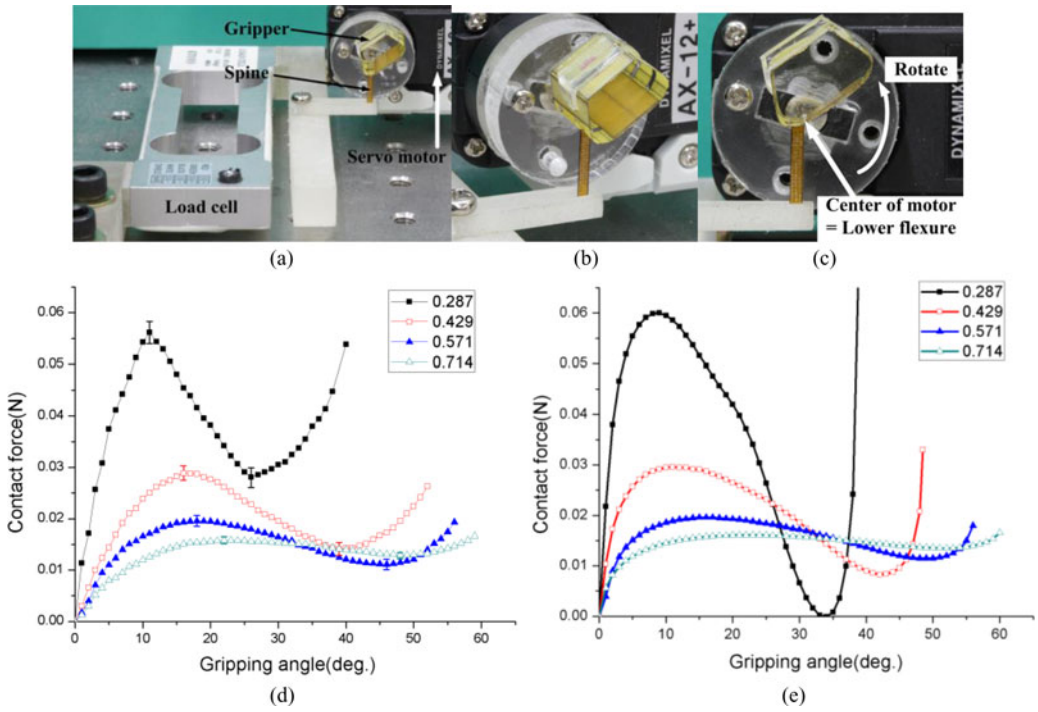

Fig. 8. (a) Experimental setup of the contact force measurement. (b) Diagonal view. (c) Magnified front view. Each gripper is fixed to the servo motor. The center of the lower flexure is fitted to the center of the motor so that the spine is always perpendicular to the bar connected to the load cell. The servo motor then rotates by 1° and measured the data after the contact force settles down to a static value. Five runs are done for each gripper with different length ratio and the error bars are indicated in the graph to show the standard deviation. The experiments are performed when 10% of the initial distance is actuated, which is the general actuation length when a gripper grips a surface. (d) Experimental and (e) simulated results for gripping angle versus contact force according to various length ratios of the middle flexure. Numbers in the legend x correspond to the ratio of the middle flexure $L_1{:}L_2{:}L_3{:}l = 1{:}x{:}0.429{:}0.057$.

TABLE IV
VALUES OF PARAMETERS OF THE GRIPPER IN THE EXPERIMENTS AND THE SIMULATIONS

Parameters	Value	Unit
L_0	4	mm
L_1	3.5	mm
L_2	1.0, 1.5, 2.0, 2.5	mm
L_3	1.5	mm
L_4	4	mm
Ls	9.8	mm
l	0.2	mm
θ_0	65	deg.

TABLE V
COMPARISON OF EXPERIMENTAL AND SIMULATION RESULTS

	Length ratio	R_G (degrees)	F_L (N)	F_V (N)
Experiment	0.287	40	0.0371	0.0126
	0.429	52	0.0194	0.0060
	0.571	55	0.0145	0.0050
	0.714	59	0.0133	0.0031
Model	0.287	38.5	0.0344	0.0224
	0.429	48.5	0.0201	0.0082
	0.571	56	0.0153	0.0039
	0.714	60	0.0142	0.0027

increases to 0.714, the *gripping range* increases to 59°, but the *force level* decreases to 0.0133 N.

The *force level* shows the average of contact forces but has difficulties to predict dispersion of the contact forces. To provide variation of the contact forces, we define the *force variation* as

$$F_V = \sqrt{\frac{1}{\theta_{\max}} \int_0^{\theta_{\max}} (F_L - f_c(\theta))^2 d\theta} \qquad (13)$$

which is the standard deviation of the contact forces. This indicates the variation of contact forces from the *force level* and the *force variation* could be a criterion to judge even contact force condition. The *force variation* decreases as the flexure becomes longer. In Fig. 8(d), in the case of the length ratio of 0.287, the *force variation* is as large as 0.0126 N. Conversely, for the gripper with the length ratio of 0.714, the corresponding value is 0.0031 N, which means the contact forces are similar without considering spine configuration.

Using the derived model, we simulated the contact force. The results are shown in Fig. 8(e) and compared with the experimental results. Table V presents a comparison of the experimental and simulation results. The simulation result and experimental result fit quite well when the flexure is long. When the flexure is short, some error is present in the *force level* and the *force variation*. In the case of short flexures, these are under high loading

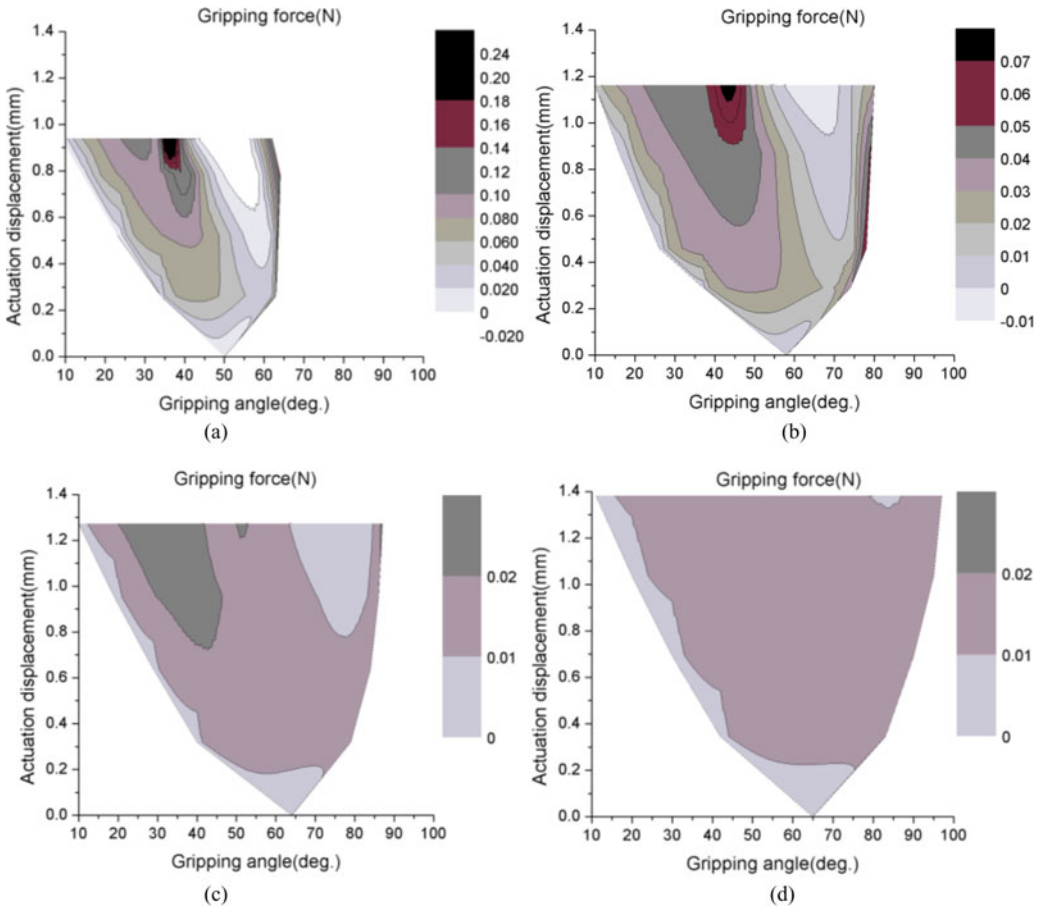

Fig. 9. Contact force according to the gripping angle and actuation displacement. Grippers with flexure lengths of (a) 0.278, (b) 0.429, (c) 0.571, and (d) 0.714 for the middle flexure are used for the simulation. The simulation is carried out when the actuation displacement is 5%, 10%, 15%, and 20% of the initial distance.

conditions, such as large axial forces that compress or place the beam under tension, and cases where the beam has inflection points imply that the beam curvature has changed; these are limitations of the proposed model. While some error occurs in short flexures, we are more interested in the long flexures that will be used in practice.

The results of the experiment give the contact force at the specified actuation displacement D as shown in Fig. 6. To predict the characteristics under other actuation displacement values, we need to simulate the characteristics under various actuation displacements using the derived model. The simulations were performed while varying the length ratio of the flexure, and the results are shown in Fig. 9. The results show the changes in the characteristics with varying actuation displacements.

Of the three characteristics, we focused on the *force variation*, since this is sensitive to the actuation displacement depending on the length of the flexure. In all cases, the *force variation* increases as the actuation displacement increases, but the extent is very different. In the case of the short flexures with length ratios of 0.287 and 0.429, the *force variation* increases steeply. When the grippers with these length ratios are fully actuated, the force variations are 0.26 and 0.08 N, respectively, as shown in Fig. 9(a) and (b). Conversely, in the case of longer flexures, a narrow *force variation* is observed. Even when the grippers are fully actuated, the force variations are only 0.02 N for the 0.571 length ratio and 0.01 N for the 0.714 length ratio. The simulation results suggest that the Buckling gripper with the long flexure ratio enables the spines to have even contact forces, regardless of actuation displacement or gripping angle.

B. Discussion

From the contact force measurements, we find that the gripper with the long flexure has a lower *force level* but a wider *gripping range* and a narrower *force variation* than the gripper with the short flexure.

The values of the three proposed parameters enable us to understand the mechanism of adaptive gripping and to determine an adequate length ratio for the flexure that satisfies the conditions of adaptive gripping: a sufficient number of contacts and even contact forces. The number of contact points at which the spines actually touch the surface is related to the *gripping range*. The *gripping range* is the actual displacement through which the each spine can move independently. Thus, a wide *gripping range* increases the probability that a spine is able to engage with asperities on the target surface; the wider the *gripping*

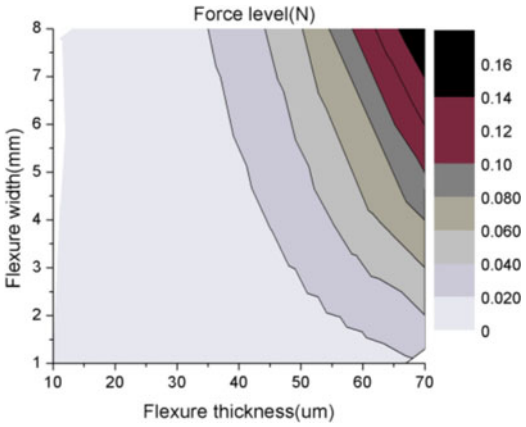

Fig. 10. Force level according to flexure thickness and flexure width.

range, the longer the displacement of scraping the asperities. Therefore, the gripper with long flexure has a high probability of overcoming a low *force level* via an increased number of contacts.

The gripper with long flexure has not only greater number of contacts but also has even contact forces exerted by the spines on the surface. When a gripper grips a surface, the actuation displacement is determined as a constant value, but each spine has its own gripping angle, depending on the shape of the target surface. The difference in the gripping angle corresponds to the difference in contact force. The narrow *force variation*, however, enables all spines to have similar contact forces, which results in a more stable gripping posture.

In addition, the simulation results help in designing a gripper that has the desired *gripping range*, *force level*, and *force variation*. The *gripping range* and the *force variation* are determined by the length ratio of the middle flexure. Based on the previous analysis, we recommend that the length ratio of the middle flexure be larger than 0.571. Furthermore, the desired *force level* can be obtained by adjusting the width and the thickness of the flexure. In the section on modeling, we showed that the *force level* is proportional to the width and the cube of the thickness. Fig. 10 shows the force level according to the flexure width and flexure thickness.

These results are obtained from the one-way gripping action. If the contact forces were measured while the gripper is being opened, however, the graph could be different because of the hysteresis effect. Therefore, in the applications where a two-way gripping action or a feedback control is required, the hysteresis effect needs to be considered.

C. Gripping Performance on Artificially Controlled Surfaces

We have shown that the gripper with the long flexure is more likely to achieve adaptive gripping. To verify the gripping performance, we performed experiments on various surfaces.

Generally, a surface has two kinds of characteristics: surface roughness and surface waviness. Roughness is a measure of the texture of a surface. For example, machined granite, polished granite, and rough-cut granite are same material but have different surface roughness. Waviness is a broader view of roughness and indicates how uneven, undulating, and rugged a surface is.

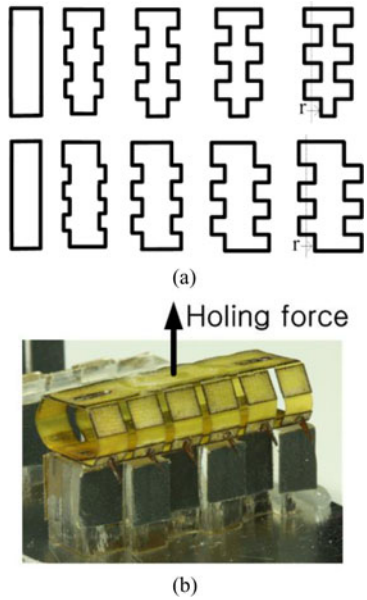

Fig. 11. (a) Symmetric blocks and asymmetric blocks with different degrees of surface waviness r that stands for undulation of the blocks. (b) Experimental setup for holding force measurements.

Overcoming surface roughness depends greatly on the tip radius of the spine and the contact angle [38]. This means that a gripper can hook most surfaces if the gripper has very sharp spines and an appropriate contact angle. However, a gripper may grip only one of two surfaces of the same roughness if they differ in waviness. Therefore, in order to not only hook but grip rugged surfaces as well, a gripper should be able to overcome surface waviness.

To exclude the influence of surface roughness as related to the tip radius of the spine, we performed an experiment with several blocks having artificially controlled roughness and waviness. The roughness of these blocks had a unique value, but the degrees of waviness were different. Therefore, we investigated the influence of only surface waviness on gripping performance.

Gripping performance was tested on two quite differently arranged blocks in order to test their performance under various conditions. One block has a symmetric arrangement and the other has an asymmetric arrangement, as shown in Fig. 11(a). To test the gripping performance depending on the length ratio of the flexure, two grippers were prepared. Both grippers had six pairs of spines each, but had different length ratios of the flexure: 0.287 and 0.571. Their performance was evaluated in terms of measurement of the holding force ratio and the holding force, as shown in Fig. 12(a). The holding force ratio is the ratio of the holding force when the waviness value is zero to when it is not zero. This ratio provides a clear comparison of the variations in the holding force caused by the surface waviness of the two grippers.

On the symmetric blocks, the holding force in the long flexure maintained 71% of the initial holding force ratio in spite of an increase in the waviness. In case of the short flexure, however,

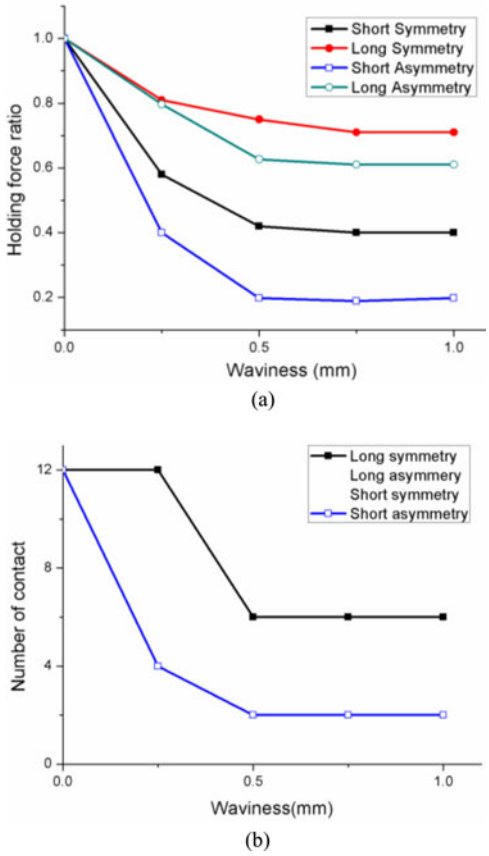

Fig. 12. (a) Holding force ratio versus waviness. (b) Number of contacts versus waviness. Cases of the long symmetry/asymmetry and the short symmetry have the same profile.

the holding force ratio rapidly decreased, and 40% of the initial holding force was maintained. This result is attributed to a decrease in the number of contacts. When the flexure is short, the number of contacts decreases rapidly, whereas it declines gradually when the flexure is long.

This phenomenon can be clearly seen in the case of the asymmetrically arranged blocks, as shown in Fig. 12. On asymmetric blocks, the gripper with the short flexures rotates and tilts, since the sum of the moments from the reaction force of the spines causes failure of the gripping. In Fig. 12(b), this phenomenon boosts the decrease in the number of contacts by leading to an unstable position. As can be seen in Fig. 12(a), the holding force ratio for the case of short symmetry decreases rapidly, and only 19% of the initial holding force ratio is maintained. In contrast, the holding force ratio for the case of long symmetry decreases modestly, and 61% of the initial holding force ratio remains. Further, the moments from the reaction forces of the spines are exerted on the gripper, but the compliance of the flexure behaves as if there were damping. As a result, the gripper hardly rotates at all and sustains a higher holding force ratio than is the case with short symmetry.

D. Gripping Performance on Natural Surfaces

In the real world, different surfaces have different surface roughness and waviness properties. To demonstrate the feasibility of the Buckling gripper under random conditions, we performed gripping tests on randomly chosen cement blocks commonly found in real life. Three cement surfaces that have similar surface roughness but different waviness properties were prepared. The aim of this was also to focus on overcoming surface waviness.

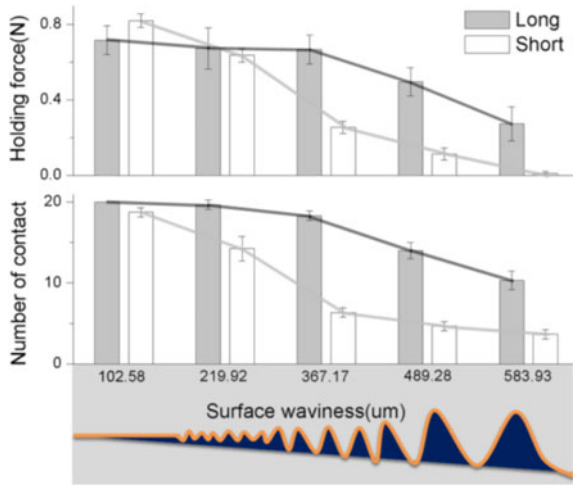

Fig. 13. Holding force versus surface waviness on randomly chosen cement surfaces. The lines and bars indicate the holding force and the number of contacts, respectively.

To verify the gripping performance according to the length of the flexure, two grippers having flexures with different length ratios were prepared. The length ratio for the middle flexure of one gripper was 0.714, and that of the other gripper was 0.287.

Evaluation was performed by measuring the holding force and checking the number of contacts. To better observe the difference in the number of contacts, each gripper was designed to have ten pairs of spines. For each block, gripping was attempted ten times.

Fig. 13 shows the results. The x-axis in these parts of the figure represents the surface waviness, and the y-axis in these parts represents the number of contacts and holding force, respectively. Both the number of contacts and the holding force decrease as the surface waviness increases, but the extent of decrease is different. In the case of short flexure, the number of contacts decreases from 18.8 to 14.3 as soon as the surface waviness increases and drops to 3.7. The holding force shows larger initial value than the longer case but drops steeply as the surface waviness changes and reaches 0 N on the fifth surface. That is, none of the spines grip. In contrast, for the gripper with long flexure, the number of contacts decreases from 20 to 18.3 when the cement surface is changed to a wavier surface. Not only does the number of contacts barely drop, but also the holding force shows only a slight decrease. Even when the cement surface is changed to the much wavier surface, the number of contacts is 10.3, and the holding force is 0.053 N. These values are much larger than those of the gripper with short flexure.

Fig. 14 shows the 140-mg Buckling gripper attached to a tree, stone, and brick with 3.0 g weight. A magnified picture of the Buckling gripper is also shown in Fig. 14(c). Depending on the

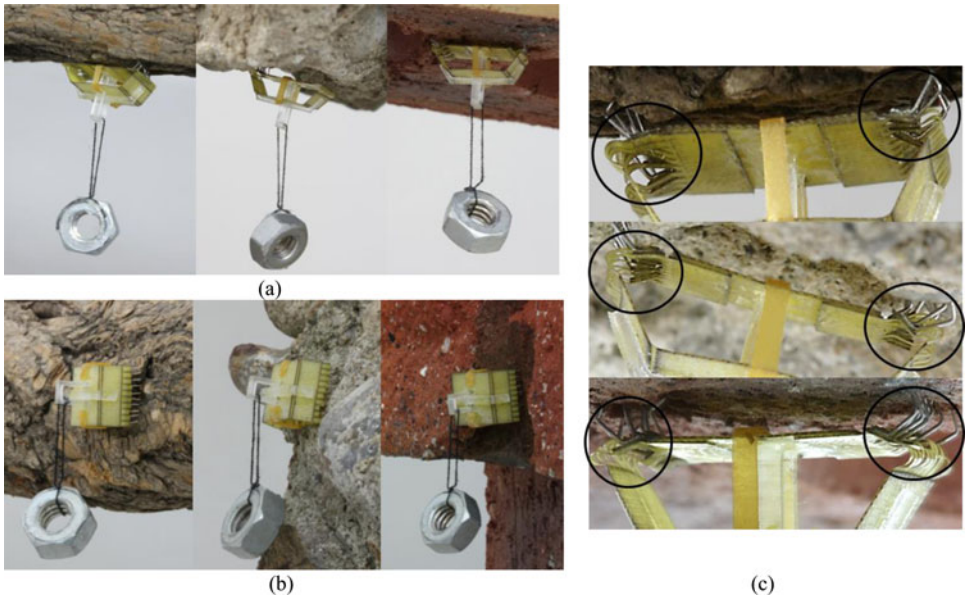

Fig. 14. (a), (b) Buckling gripper attached to a tree, stone, and brick. (c) Magnified images of (a).

shape of the surface, each spine deforms by different amounts (circles in Fig. 12) and attaches to the target surfaces adaptively.

VI. Conclusion

We have proposed a novel type of adaptive gripper called the Buckling gripper. The Buckling gripper achieves adaptive gripping on uneven, rugged, and undulating surfaces. The key design principle is flexural buckling, which has been inspired by nature. Using the PRBM model, we showed that the buckling behavior of the middle flexure with a suitably chosen length ratio provides not only a wide gripping range but a narrow range of force variation as well. As a result, these properties contribute to an increase in the number of contacts with even contact forces. The actual effects of the flexural buckling were verified by carrying out gripping performance tests on randomly chosen cement blocks commonly found in the real world.

We expect the gripper to be used in small-scale applications. In particular, it has significant advantages when employed in small-scale mobile robots that maneuver in hazardous situations where numerous cracks or potholes exist or climbs undulating surfaces for search and rescue. In these situations, the robot is required to maintain tight grip on rough and wavy surfaces. In small scale, to employ gripping devices with additional underactuated mechanisms is challenging since such mechanisms tend to be weighty and cause the robots to be complicated. Due to the simplicity of the mechanism proposed, the entire system becomes lightweight and easy to fabricate. We previously have shown the feasibility by applying the early version of the Buckling gripper to a small-scale crawling robot [39] that has a finger size dimension and a weight of 1.2 g. The robot is inspired by an inchworm and has one gripper to grip the ground and lift its body on one end. It can swing the upper body to explore the surroundings. This crawling robot can be extended to a climbing robot by employing two grippers at both ends. The robot will be able to climb walls by alternatively gripping and releasing each gripper. In addition, to increase the successful gripping probability, segments of the *spine link* need to be increased. Other examples that use spines, e.g., Spinybot [11] and omnidirectional anchor [15], have large number of spines to increase the number of contacts and load sharing ability. Similarly, the Buckling gripper can increase the successful gripping probability and the holding force by increasing the number of the *spine links*.

In the future, diversifying the shapes of the gripper and increasing the number of *spine links* will provide better gripping performance, e.g., circular shape with *spine links* on all edges. Furthermore, the scalability of the mechanism will enable us to expand the field of applications by providing a hand size gripper that can grasp variously shaped objects such as cups and phones.

References

[1] L. Birglen, C. Gosselin, and T. Laliberté, *Underactuated Robotic Hands*. vol. 40, New York, NY, USA: Springer-Verlag, 2008.
[2] S. Hirose and Y. Umetani, "The development of soft gripper for the versatile robot hand," *Mech. Mach. Theory*, vol. 13, no. 3, pp. 351–359, 1978.
[3] N. Fukaya, S. Toyama, T. Asfour, and R. Dillmann, "Design of the TUAT/Karlsruhe humanoid hand," in *Proc. IEEE/RSJ Int. Conf. Intell. Robots Syst.*, 2000, vol. 3, pp. 1754–1759.
[4] M. Kaneko, M. Higashimori, R. Takenaka, A. Namiki, and M. Ishikawa, "The 100 G capturing robot-too fast to see," *IEEE/ASME Trans. Mechatronics*, vol. 8, no. 1, pp. 37–44, Mar. 2003.
[5] M. C. Carrozza, C. Suppo, F. Sebastiani, B. Massa, F. Vecchi, R. Lazzarini, M. R. Cutkosky, and P. Dario, "The SPRING hand: Development of a self-adaptive prosthesis for restoring natural grasping," *Autonom. Robots*, vol. 16, no. 2, pp. 125–141, 2004.
[6] B. Massa, S. Roccella, M. C. Carrozza, and P. Dario, "Design and development of an underactuated prosthetic hand," in *Proc. IEEE Int. Conf. Robot. Autom.*, 2002, vol. 4, pp. 3374–3379.
[7] C. Gosselin, F. Pelletier, and T. Laliberte, "An anthropomorphic underactuated robotic hand with 15 Dofs and a single actuator," in *Proc. IEEE Int. Conf. Robot. Autom.*, 2008, pp. 749–754.
[8] H. K. In, K. J. Cho, K. R. Kim, and B. S. Lee, "Jointless structure and under-actuation mechanism for compact hand exoskeleton," in *Proc. IEEE Int. Conf. Rehab. Robot.*, 2011, pp. 1–6.

[9] A. M. Dollar and R. D. Howe, "The highly adaptive SDM hand: Design and performance evaluation," *Int. J. Robot. Res.*, vol. 29, no. 5, pp. 585–597, 2010.
[10] R. Volpe, J. Balaram, T. Ohm, and R. Ivlev, "The rocky 7 mars rover prototype," in *Proc. IEEE/RSJ Int. Conf. Intell. Robots Syst.*, 1996, vol. 3, pp. 1558–1564.
[11] S. Kim, M. Spenko, S. Trujillo, B. Heyneman, D. Santos, and M. R. Cutkosky, "Smooth vertical surface climbing with directional adhesion," *IEEE Trans. Robot.*, vol. 24, no. 1, pp. 65–74, Feb. 2008.
[12] S. Kim, A. T. Asbeck, M. R. Cutkosky, and W. R. Provancher, "SpinybotII: Climbing hard walls with compliant microspines," in *Proc. Int. Conf. Adv. Robot.*, 2005, pp. 601–606.
[13] F. Lotti, P. Tiezzi, G. Vassura, L. Biagiotti, G. Palli, and C. Melchiorri, "Development of UB hand 3: Early results," in *Proc. IEEE Int. Conf. Robot. Autom.*, 2005, pp. 4488–4493.
[14] S. Kota, K. J. Lu, K. Kreiner, B. Trease, J. Arenas, and J. Geiger, "Design and application of compliant mechanisms for surgical tools," *J. Biomech. Eng.*, vol. 127, no. 6, pp. 981–989, 2005.
[15] A. Parness, "Anchoring foot mechanisms for sampling and mobility in microgravity," in *Proc. IEEE Int. Conf. Robot. Autom.*, 2011, pp. 6596–6599.
[16] [Online]. Available: http://www.festo.com/cms/en_corp/9779.htm
[17] E. Brown, N. Rodenberg, J. Amend, A. Mozeika, E. Steltz, M. R. Zakin, H. Lipson, and H. M. Jaeger, "Universal robotic gripper based on the jamming of granular material," *Proc. Natl. Acad. Sci. U.S.A.*, vol. 107, no. 44, pp. 18809–18814, 2010.
[18] F. Ilievski, A. D. Mazzeo, R. F. Shepherd, X. Chen, and G. M. Whitesides, "Soft robotics for chemists," *Angew. Chem.*, vol. 123, no. 8, pp. 1930–1935, 2011.
[19] N. Dechev, W. L. Cleghorn, and J. K. Mills, "Microassembly of 3-D microstructures using a compliant, passive microgripper," *J. Microelectromech. Syst.*, vol. 13, no. 2, pp. 176–189, 2004.
[20] M. N. M. Zubir, B. Shirinzadeh, and Y. Tian, "Development of a novel flexure-based microgripper for high precision micro-object manipulation," *Sens. Actuators, A: Phys.*, vol. 150, no. 2, pp. 257–266, 2009.
[21] F. Krecinic, T. C. Duc, G. K. Lau, and P. M. Sarro, "Finite element modelling and experimental characterization of an electro-thermally actuated silicon-polymer micro gripper," *J. Micromech. Microeng.*, vol. 18, no. 6, p. 064007, 2008.
[22] B. Hoxhold and S. Büttgenbach, "Easily manageable, electrothermally actuated silicon micro gripper," *Microsyst. Technol.*, vol. 16, no. 8, pp. 1609–1617, 2010.
[23] F. Beyeler, A. Neild, S. Oberti, D. J. Bell, Y. Sun, J. Dual, and B. J. Nelson, "Monolithically fabricated microgripper with integrated force sensor for manipulating microobjects and biological cells aligned in an ultrasonic field," *J. Microelectromech. Syst.*, vol. 16, no. 1, pp. 7–15, 2007.
[24] R. E. Snodgrass, *Principles of Insect Morphology*. New York, NY, USA: McGraw–Hill, 1935.
[25] J. H. Belanger and B. A. Trimmer, "Combined kinematic and electromyographic analyses of proleg function during crawling by the caterpillar Manduca sexta," *J. Comp. Physiol. A: Neuroethology, Sensory, Neural, Behavioral Physiol.*, vol. 186, no. 11, pp. 1031–1039, 2000.
[26] R. F. Chapman, *The Insects: Structure and Function*. Cambridge, U.K.: Cambridge Univ. Press, 1998.
[27] L. L. Howell, *Compliant Mechanisms*. New York, NY, USA: Wiley-Interscience, 2001.
[28] L. L. Howell and A. Midha, "Parametric deflection approximations for end-loaded, large-deflection beams in compliant mechanisms," *J. Mech. Des.*, vol. 117, pp. 156–165, 1995.
[29] A. Saxena and S. N. Kramer, "A simple and accurate method for determining large deflections in compliant mechanisms subjected to end forces and moments," *J. Mech. Des.*, vol. 120, pp. 392–400, 1998.
[30] L. Saggere and S. Kota, "Synthesis of planar, compliant four-bar mechanisms for compliant-segment motion generation," *J. Mech. Des.*, vol. 123, pp. 535–541, 2001.
[31] H. J. Su, "A pseudorigid-body 3R model for determining large deflection of cantilever beams subject to tip loads," *J. Mech. Robot.*, vol. 1, no. 2, pp. 021008-1–021008-9, 2009.
[32] R. J. Wood, S. Avadhanula, R. Sahai, E. Steltz, and R. S. Fearing, "Microrobot design using fiber reinforced composites," *J. Mech. Des.*, vol. 130, pp. 052304-1–052304-11, 2008.
[33] K. J. Cho, J. S. Koh, S. Kim, W. S. Chu, Y. Hong, and S. H. Ahn, "Review of manufacturing processes for soft biomimetic robots," *Int. J. Precis. Eng. Manuf.*, vol. 10, no. 3, pp. 171–181, 2009.
[34] M. Noh, S. W. Kim, S. An, J. S. Koh, and K. J. Cho, "Flea-inspired catapult mechanism for miniature jumping robots," *IEEE Trans. Robot.*, vol. 28, no. 5, pp. 1007–1018, Oct. 2012.
[35] J. S. Koh and K. J. Cho, "Omega-shaped inchworm-inspired crawling robot with large-index-and-pitch (LIP) SMA spring actuators," *IEEE/ASME Trans. Mechatronics*, vol. 18, no. 2, pp. 419–429, Apr. 2013.
[36] S. M. An, J. Ryu, M. Cho, and K. J. Cho, "Engineering design framework for a shape memory alloy coil spring actuator using a static two-state model," *Smart Mater. Struct.*, vol. 21, no. 5, p. 055009, 2012.
[37] G. P. Jung, J. S. Koh, and K. J. Cho, "Meso-scale compliant gripper inspired by caterpillar's proleg," in *Proc. IEEE Int. Conf. Robot. Autom.*, 2011, pp. 1831–1836.
[38] A. T. Asbeck, S. Kim, M. R. Cutkosky, W. R. Provancher, and M. Lanzetta, "Scaling hard vertical surfaces with compliant microspine arrays," *Int. J. Robot. Res.*, vol. 25, no. 12, pp. 1165–1179, 2006.
[39] J. Koh and K. Cho, "Omegabot: Crawling robot inspired by ascotis selenaria," in *Proc. IEEE Int. Conf. Robot. Autom.*, 2010, pp. 109–114.

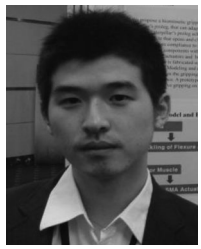

Gwang-Pil Jung (S'11) received the B.S. degree in mechanical engineering from the Korea Advanced Institute of Science and Technology, Daejeon, Korea, in 2010. He is currently working toward the Ph.D. degree in mechanical engineering with the Biorobotics Laboratory, Seoul National University, Seoul, Korea.

His current research interests include the design and fabrication of biologically inspired robots and novel mechanisms using smart materials, structures, and actuators.

Mr. Jung received a Fourth-Place Award in the Student Mechanism and Design Competition at the ASME International Design Engineering Technical Conferences in 2012.

Je-Sung Koh (S'10) received the B.S. degree in mechanical and aerospace engineering from Seoul National University, Seoul, Korea, in 2008, where he is currently working toward the Ph.D. degree with the Biorobotics Laboratory.

His current research interests include bioinspired robot design and small-scale robot design with smart materials and actuators.

Mr. Koh received the Best Student Paper Award at the IEEE/Robotics Society of Japan IEEE Engineering in Medicine and Biology Society International Conference on Biomedical Robotics and Biomechatronics in 2010.

Kyu-Jin Cho (M'08) received the B.S. and M.S. degrees from Seoul National University, Seoul, Korea, in 1998 and 2000, respectively, and the Ph.D. degree in mechanical engineering from the Massachusetts Institute of Technology, Cambridge, MA, USA, in 2007.

He was a Postdoctoral Fellow with Harvard Microrobotics Laboratory, Cambridge, until 2008. He is currently an Associate Professor of mechanical and aerospace engineering and the Director of the Biorobotics Laboratory, Seoul National University. His research interests include biologically inspired robotics, robotic systems using smart actuators, novel mechanisms using smart structures, and rehabilitation and assistive robotics.